RSC Advances




ROYAL SOCIETY OF CHEMISTRY

www.rsc.org/advances

Cite this: DOI: 10.1039/c0xx00000x

www.rsc.org/xxxxxx

# Communication

# Corrosion and wear Resistance of 32CrMoV13 Steel Nitrided by Plasma

**Okba Belahssen,[a] Abdelouahed Chala,[a] Hachemi Ben Temam,[a] Said Benramache,[b,] ***

***Received (in XXX, XXX) Xth XXXXXXXXX 20XX, Accepted Xth XXXXXXXXX 20XX***
**DOI: 10.1039/b000000x**

**This paper presents corrosion and wear behavior of the plasma-nitrided 32CrMoV13 steel. Untreated and plasma nitrided samples were tested. The structure of layers was determined by X–ray diffraction, the morphology was observed by scanning electron microscopy (SEM). The corrosion behavior was evaluated by electrochemical techniques (potentiodynamic curves and electrochemical impedance spectroscopy). The corrosion tests were carried out in acid chloride solution (HCl 1M). The plasma nitriding behaviors of 32CrMoV13 steel have been assessed by evaluating tribological properties and surface hardness by using a pin–on–disk wear machine and microhardness tester. Experimental results showed that the nitrides ε–$Fe_2$–3N and γ′–$Fe_4$N present in the white layer are nobler than the substrate but may promote, by galvanic effect, a localized corrosion through open porosity. The better corrosion protection was observed for nitrided sample. It is found that plasma nitriding improves the wear rate, and the presence of a hard and brittle compound layer on the surface causes an increase in wear of specimen surface.**

Plasma nitriding is a thermochemical process extensively applied in metallic materials science and surface engineering due to its well-known potential for improving properties such as hardness, wear, and corrosion resistance of metallic parts [1,2]. This surface treatment technique consists of the implantation of nitrogen species at low energies into the steel substrate and their subsequent diffusion into the bulk at temperatures above 300 °C. The interaction of nitrogen and steel constituents leads to the formation of different types of metallic nitrides, which form the so–called ‘‘nitride layer”. Starting from the solid surface, such a modified layer usually comprises an oxide layer, a compound zone and a diffusion zone [3,4]. The resulting structure of these domains depends on several processing parameters such as the concentration of alloying elements, exposure time, substrate temperature and gaseous mixture [5,6]. The presence of a nitride layer obviously changes the mechanisms of interaction between metallic materials and their surroundings, thus affecting their stability in aggressive environments [7–9]. The incorporation of nitrogen imparts better mechanical properties (friction and wear resistance) [10], but the dissolution kinetics (corrosion resistance) remains closely related to the composition of the corrosive medium [11,12].

In this context, the 32CrMoV13 steel is largely employed in industrial processes that take place in aggressive environments. Hard iron nitrides are originated during the plasma treatment owing to nitrogen diffusion in the near surface region at temperatures below the eutectic point (593 °C) [13]. Usually, two distinctive phases corresponding to the ε–$Fe_2$–3N and γ’–$Fe_4$N nitrides are obtained, whose high hardness improves the strength, friction and wear resistance [14,15]. However, the highest wear resistance is normally achieved when the close–packed hexagonal ε–$Fe_2$–3N phase is primarily at the surface of the specimens. This is so because the mixed nitride layer of the ε–$Fe_2$–3N and γ’–Fe4N phases is, in fact, stressed due to a crystal lattice mismatch [16–19].

Recent work have shown that the pitting corrosion resistance of the steel can be significantly improved by nitride layers consisting of ε–$Fe_2$–3N and γ’–$Fe_4$N phases [20,21]. However, the effect of the nitride layer microstructure on the pitting corrosion behaviour of steel is still not fully understood. In this study, we address this question by analysing the influence of plasma processing at optimal parameters (temperature 500 °C, exposure time 4h and gaseous mixture 20 % $H_2$, 80% $N_2$) [22] on the corrosion, wear behaviour and microstructure of plasma-nitrided 32CrMoV13 steel.

32CrMoV13 steel samples with nominal composition of 94.9 % Fe, 0.3 % C, 0.31 % Si, 0.5 % Mn, 3.25 % Cr, 0.44 % Mo, 0.11 % Ni, and 0.1 % V (wt. %) were used in this study. Before plasma nitriding, samples were polished with diamond powder and ultrasonically cleaned in ethanol and during the heating step to reach the processing temperature; the specimens were ion–bombarded for 4 hours in Ar/$H_2$ 80/20 (v/v) plasma for cleaning purposes. Specimens were nitrided in a vacuum furnace pumped down to low pressure (3 mbar) to minimize the oxygen contamination. The temperature of the samples is measured with the use of a thermocouple. The nitriding parameters were fixed similar to previous works [23]. After processing, the samples were left to cool down slowly (during 8 hours) inside a vacuum chamber.

[a]*Laboratoire de Physique des Couches Minces et Application, Biskra University, Biskra 07000, Algeria*
[b]*Materials Science Department, Faculty of Sciences, Biskra University, Biskra 07000, Algeria. E-mail: saidbenramache07@gmail.com*

The morphology of the samples surfaces was observed by Jeol 5900 Scanning Electron Microscope (SEM). Xray diffraction analyses with Co Kα monochromatic radiations were performed to determine their structure. The samples for XRD and SEM analyses were mirror–polished with colloidal silica (mesh size = 0.05 µm). The nitrided layers were revealed at room temperature by chemical etching with Nital (2 % v/v nitric acid in absolute ethanol). The crystallographic structure of the phases was determined by XRD analysis. The diffractograms were recorded at room temperature using the Bragg–Brentano geometry.

The corrosion behaviour of nitrided alloy was evaluated by electrochemical impedance spectroscopy (EIS) measurements. Impedance data for 30 minutes of immersion were acquired by a potentiostat (AUTOLAB PGSTAT 30) and a frequency response analyzer system operating at open circuit potential in a frequency range from 100 kHz to 10 Hz with a perturbation of ± 10 mV. Experiments were conducted in a classical three electrodes cell. A saturated calomel reference electrode was used as reference electrode and a platinum (Pt) wire as counter electrode. Wear tests were carried out with a pin-on-disk tester, using a 5 mm diameter 100C6 steel ball as the pin. Unlubricated wear tests were performed at room temperature (≈ 20 °C) with a relative humidity of about 25 %, a rotation speed of 60 rpm, a normal load of 5 N and a wear track diameter of 3 mm. The wear rate is determined using the Archard equation (Eq. (1)):

$$Ku = \frac{Vu}{F_N.D} \quad (1)$$

$K_u$ is the wear rate ($m^3N^{-1}m^{-1}$); $V_u$ is the wear volume ($m^3$); $F_N$ is the applied normal force (N) and $D$ is the sliding distance (m).

The wear volume was calculated by measuring the mass lost. After the wear tests, the worn regions were examined using a Jeol 5900 SEM.

The morphology and microstructure of nitrided layers produced on near-surface regions of 32CrMoV13 steel by plasma treatment at temperature of 500 °C and exposure time 4 hours and gaseous mixture of 20 % $H_2$ and 80 % $N_2$ were determined by SEM and XRD, respectively. SEM images can reveal up to two distinct types of surface layers. SEM micrograph of cross–sections of sample plasma nitrided in Fig. 1 shows two distinct layers. One can see an outermost layer well–known as compound layer or white layer, and below it there is a modified region also known as diffusion layer [23].

The XRD diffractograms are shown in Fig. 2. Three diffraction peaks were observed at 2θ = 53.0°, 78° and 100° for the untreated 32CrMoV13 substrates, which was attributed to the α–ferrite phase. After plasma nitriding, the ε–$Fe_2$–3N phase with characteristic diffraction peaks at 2θ = 44.3°, 52.0°, 84.6° and 103.6° was identified for the whole temperature range investigated in this study. The diffractogram also revealed the appearance of diffraction peaks at 2θ = 48.0° and 56.6°, which are associated to the presence of γ'–$Fe_4N$ phase in the modified layer [23]. However, the set of diffraction peaks identified in this study clearly indicates the formation of the γ'–$Fe_4N$ phase at the steel surface. These results are consistent with the precipitation of ε–$Fe_2$–3N and γ'–$Fe_4N$ phases, thus producing the compact compound layer identified by SEM (see Fig. 1).

Fig. 3 shows the potentiodynamic polarization curves in HCl solution for the samples untreated and nitrided. After nitriding, the corrosion potential of the alloy changed from –0.506 to –0.406 mVSCE, and lower anodic current densities than for the untreated alloy, indicating an increase in the corrosion resistance, probably associated with the formation of the compound layer composed by $Fe_2$–3N and $Fe_4N$ and/or to the enrichment of the metallic matrix in nitrogen.

Electrochemical impedance spectroscopy (EIS) experiments obtained at open circuit potential (OCP) in HCl solution were performed to characterize both the untreated and nitrided 32CrMoV13 samples. Figs. 4a, 4b and 4c show the Nyquist and Bode plots of experimental data of the alloy. The nitrided sample shows a different behaviour due to the presence of nitrides with high chemical inertia. The high impedance values and phase angle of almost –60° at intermediate frequencies are indicative of a near capacitive response related to surface nitrides, evidence metallographically in Fig. 1 and by the X–ray patterns shown in Fig. 2. Moreover, a high impedance of nitrided sample confirms the low reactivity of the nitride alloy.

The results for nitrided samples can be interpreted in terms of two times constant overlapped for a broad frequency range, as also reported in recent works [24–26]. The electrochemical behaviour for 32CrMoV13 untreated was modelled by the equivalent circuit shown in Fig. 5a which is composed by circuit elements: $R_e$, representing the solution ohmic resistance between the working and the reference electrodes, $Q_1$ element, which represents a constant phase element (CPE) and describes a non–ideal capacitor when the capacitor phase angle is different from –90° [27]. CPE impedance is generally attributed to distributed surface reactivity, surface heterogeneity and roughness, to current and potential distribution related to the electrode geometry and porosity [28].

Regarding to the Nyquist plots, it is obvious that the semi circles are depressed therefore, in these models constant phase elements (CPE) is used for more accurately analysing of impedance behavior of the electric double layer. Equivalent circuit befor the treatment differs with equivalent circuit after nitiding. This is because of the change in the surface condition of sample before and after reatment.

The impedance of CPE is presented in Eq. (2). CPE can describe several behaviors: $a$=1, represents a perfect capacitance, $a$=0.5 represents a Warburg element and $a$=0 represents a resistance [29].

$$Z_{CPE} = \frac{1}{Q(J\omega)^a} \quad (2)$$

where $Q$ is the magnitude of the CPE; $\omega$ the angular frequency; $a$ as the deviation parameter which is dependent on the surface morphology.

For all circuits, the double layer capacitance (C) can be calculated from CPE parameter values Q and a using the following expression [30].

$$C = Q^{\frac{1}{a}} R^{\frac{1-a}{a}} \quad (3)$$

In Fig. 5a the equivalent circuit is composed by elements: Re (the solution ohmic resistance), element $R_1$ corresponds to the polarization resistance which is related to the charge transfer resistance at the metal/solution interface. $W$ element is the



 

Warburg impedance, which results in the resolution of general diffusion equations considering the semi-infinite linear diffusion. The treated sample was modelled as also proposed in the recent work [26], by the equivalent circuit shown in Fig. 5b which is composed by elements: Re (the solution ohmic resistance), $Q_1$ and $Q_2$ elements, which represent a $CPE_1$ and $CPE_2$ respectively, R1 (resistance of the porous nitride layer), $R_2$+$R_3$ (the charge transfer resistance at the metal/nitide interface). On the Nyquist plot (Fig. 4a); an inductive loop appears at low frequencies. The existence of a second semi-circle is attributed to an adsorption of the reaction products on the electrode and the change in solution concentration phenomenon.

The values of equivalent circuit elements resulting from simulation by the EC–Lab 10.02 software are shown in Table 1 for the untreated sample and the nitrided one. The results reveal that there is a significant increase in passivity resistance ($R_1$). This parameter has value of 25.4 $\Omega.cm^2$ of untreated sample to 49.11 $\Omega.cm^2$ of the nitrided alloy. The reason for this notable increase in passivity resistance is the increase in the passivity nitride layer.

The phase–angle profiles in the low frequency region in Fig. 4c confirm the predominant capacitive contribution on nitrided sample, maintaining high θ values for frequencies much lower than for the untreated alloy. All these features point to a higher corrosion resistance of the nitrided sample than of the untreated sample. The fitted curves are shown in Fig. 6a for the untreated sample and Fig. 6b for the nitrided one.

On the surfaces of untreated sample we see considerable damage following the attack particularly strong of hydrochloric acid (see Fig. 7a), by against the nitrided samples (see Fig. 7b) the corrosion behavior was different, the nitrided layers are compact and do not reveal cracks that could allow direct contact between the substrat and the solution.

Fig. 8 shows microhardness profile of sample treated at 500 °C for 4 hours of treatment time at 80/20 of $N_2$–$H_2$ gas mixture. Microhardness profile obtained from cross-section of treated specimen show the presence of a slope interface between the case (nitrided layer) and the core. Higher surface hardness values and big depth are obtained at these conditions. These results are in good accordance with those of Krishnaraj et al. [31] who studied the mechanical properties of plasma nitrided steel. Priest and al. [32] studied the effect of hydrogen in the case of nitriding to low pressure of steels they showed that hydrogen have an effect on the diffusion of nitrogen. The surface hardness of 32CrMoV13 steel was increased up to two times by the plasma nitriding process [33].

In this study, the friction reduction and anti–wear properties on the untreated surface were compared with those on the nitrided surface. The friction coefficients measured against a 100C6 steel ball are shown in Fig. 9a for the plasma nitrided specimen and untreated one. It was observed in each case that the friction coefficient rose to a steady value during the test time. The steady values of the friction coefficients are approximately between 0.4 for the nitrided sample and 0.8 for the untreated one indicates that the presence of a compound layer with very good friction characteristics caused even lower values of the friction coefficient. However, the plasma nitrided steel presents the lowest wear rates (Fig. 9b). This behavior could be explained by the hardness of the materials which is 1050 HV at the surface. The increase in wear rate is inversely proportional to the decrease in hardness values of the materials. The presence of a hard and brittle compound layer on the surface caused an increase in the wear of specimen surface due to the fracture of the compound layer with high stress and formation of hard, abrasive particles in the initial stage of sliding.

It can be seen that the prevailing wear mechanism is adhesive wear, which is found for all nitrided specimens. However, the presence of a compound layer causes the appearance of an abrasion wear component because the compound layer breaks down during sliding and forms hard, abrasive particles (Fig. 10). Steel studied has undergone plastic deformation (shear asperities), causing abrasive wear also verified by other authors [34,35].

Fig. 10b shows a wear track with a compound layer. In the initial period of sliding, the brittle compound layer with high stress fractured and then transformed abrasive particles. Higher magnification reveals that this layer initially cracked and then broke into pieces. Fig. 10a illustrates the wear track without the compound layer. The wear track is shallower, uniformly stretched along the specimen surface compared to the treated sample and the wear debris is not observed besides the wear track.

In this work, it was shown that nitriding treatment applied to carbon steel enriched in chromium is adapted to the protection against corrosion of the 32CrMoV13 steel. It has been shown that both of the nitrides ε–$Fe_2$–3N and γ′–$Fe_4N$ are formed after nitriding in optimal plasma treatment conditions (temperature 500 °C, time of treatment 4 hours and gas in the mixture 20 % $H_2$ – 80 % $N_2$) and electrochemical tests confirms that nitrided layer provides good corrosion protection in HCl solution. The nitrided sample shows a significant increase in corrosion resistance.

The compound layer increases the resistance wear of steel because the presence of a hard and brittle compound layer on the surface which is due to the fracture of the compound layer with high stress and hard, abrasive particle formation in the initial stage of sliding. However, the wear rate was reduced in the cases that do not include a compound layer.

## References


1 C. Blawert, A. Weisheit, B.L. Mordike, F.M. Knoop, Surf. Coat. Technol., 1996, **85**, 15.
2 K.T. Rie, Surf. Coat. Technol., 1999, **112**, 56.
3 L.C. Gontijo, R. Machado, E.J. Miola, L.C. Casteletti, P.A.P. Nascente, Surf. Coat. Technol., 2004, **183**, 10.
4 C.A. Figueroa, F. Alvarez, J. Appl. Phys., 2004, **96**, 7742.
5 M. Hudis, J. Appl. Phys., 1973, **44**, 1489.
6 T. Czerwiec, N. Renevier, H. Michel, Surf. Coat. Technol., 2000, **131**, 267.
7 M.K. Lei, X.M. Zhu, J. Electrochem. Soc., 2005, **152**, B291.
8 R.F.A. Jargelius-Pettersson, Corros. Sci., 1999, **41**, 1639.
9 C.X. Li, T. Bell, Corros. Sci., 2006, **48**, 2036.
10 B. Podgornik, J. Vizintin, V. Leskovsek, Surf. Coat. Technol., 1998, **108**, 454.
11 J. Flis, M. Kuczynska, J. Electrochem. Soc., 2004, **151**, B573.
12 M.K. Lei, Z.L Zhang, J. Vac. Sci. Technol., 1997, **A15**, 421.
13 T. Bell, Y. Sun, A. Suhadi, Vacuum., 2000, **59**, 14.
14 T. Liapina, A. Leineweber, E.J. Mittemeijer, W. Kockelmann, Acta Mater., 2004, **52**, 173.
15 J.M.D. Coey, P.A.I. Smith, J. Magn. Magn. Mater., 1999, **200**, 405.
16 T. Bell, Heat Treat. Met., 1975, **2**, 39.
17 A. Wells, J. Mater. Sci., 1985, **20**, 2439.

18 R.L.O. Basso, C.A. Figueroa, L.F. Zagonel, H.O. Pastore, D. Wisnivesky, F. Alvarez, Plasma Process. Polym., 2007, **4S1**, S728.
19 A. Suhadi, C.X. Li, T. Bell, Surf. Coat. Technol., 2006, **200**, 4397.
20 L.L.G. da Silva, M. Ueda, R.Z. Nakazato, Surf. Coat. Technol., 2007, **201**, 8291.
21 R.L.O. Basso, R.J. Candal, C.A. Figueroa, D. Wisnivesky, F. Alvarez, Surf. Coat. Technol., 2009, **203**, 1293.
22 O. Belahssen, A. Darssouni, A. Chala, Ann. Chim. Sci. Mat., 2008, **33**, 423.
23 O. Belahssen, A. Darssouni, A. Chala, Physical & Chemical News, 2009, **47**, 84.
24 V.A. Alves, R.Q. Reis, I.C.B. Santos, D.G. Souza, F. Gonçalves, T.P. Silva, A. Rossi, L.A. Silva, Corros. Sci., 2009, **51**, 2473.
25 M. Songür, H. Celikkan, F. Gomese, A.A. Sinkel, N.S. Altun, M.L. Aksu, J. Appl. Electrochem., 2009, **39**, 1259.
26 S. Rossi, L. Fedrizzi, T. Bacci, G. Pradelli, Corros. Sci., 2003, **45**, 511.
27 G.W. Walter, Corros. Sci., 1986, **26**, 681.
28 M.F. Montemor, M.G.S. Ferreira, Electrochim. Acta, 2007, **52**, 7486.
29 N.S. Ayati, S. Khandandel, M. Momeni, M.H. Moayed, A. Davoodi, M. Rahimizadeh, Mater. Chem. Phys., 2011, **126**, 873.
30 B. Hirschorn, M.E. Orazem, B. Tribollet, V. Vivier, I. Frateur, M. Musiani, Electrochim. Acta, 2010, **55**, 6218.
31 N. Krishnara, P. Srinivasan, K.J.L. Iyer, S. Sundaresan, Wear, 1998, **215**, 123.
32 J.M. Priest, M.J. Baldwin, M.P. Fewell, Surf. Coat. Tech., 2011, **145**, 152.
33 O. Belahssen, A. Chala, S. Benramache, IJE Transactions A: Basics Vol., 2014, **27**, 621.
34 L. Avril, Elaboration de revêtements sur acier inoxydable simulation de la fusion par irradiation laser caractérisation structurale, mécanique et tribologique, thèse de doctorat l'école nationale supérieure d'arts et métiers, Angers France, 2003.
35 A. Shafiee, M. Nili-Ahmadabadi, H.M. Ghasemi, E. Hossein-Mirzaei, International Journal of Material Forming, 2009, **2**, 237.


**Table 1**

| | Untreated sample (fig.5a) | Nitrided sample (fig.5b) |
|---|---|---|
| $R_e$ ($\Omega cm^2$) | 1.554 | 4.446 |
| $Q_1$ ($\mu F.cm^{-2}.s^{a-1}$) | 1640.0 | 283.2 |
| $a_1$ | 0.7388 | 0.8528 |
| $C_1$ ($\mu Fcm^{-2}$) | 533.3 | 74.06 |
| $R_1$ ($\Omega.cm^2$) | 25.4 | 49.11 |
| $Q_2$ ($\mu F.cm^{-2}.s^{a-1}$) | - | 196.0 |
| $a_2$ | - | 0.9215 |
| $C_2$ ($\mu Fcm^{-2}$) | - | 51.22 |
| $R_2$ ($\Omega.cm^2$) | - | 15.44 |
| $R_3$ ($\Omega.cm^2$) | - | 19.78 |
| L (H) | - | 15.01 |
| W ($\Omega.cm^2s^{-0,5}$) | 23.20 | - |

## Tables and Figures captions

**Table 1.** Obtained results of EIS method, for untreated and itrided 32CrMoV13 in 1 M HCl solution.

**Fig. 1.** SEM micrograph of 32CrMoV13 steel surface after plasma nitriding for 4 h at 500 °C in gas mixture 20% H2, 80% N2.

**Fig. 2.** XRD patterns of 32CDV13 steel surface after plasma nitriding for 4 h at 500 °C in gas mixture 20% H2, 80% N2.

**Fig. 3.** Potentiodynamic polarization curves in HCl solution for untreated

**Fig. 4.** Nyquist and Bode plots of experimental data of untreated and nitrided alloy.

**Fig. 5.** Equivalent circuits which are used for modeling the EIS results: (a) untreated sample, (b) nitrided sample.

**Fig. 6.** Experimental and fitted curves: (a) untreated sample, (b) nitrided sample

**Fig. 7.**The SEM morphologies after corrosion tests: (a) untreated sample, (b) nitrided sample.

**Fig. 8.** Variation of the microhardness according to the depth.

**Fig. 9.** a) Friction coefficient patterns and b) Wear rate constant of 32CrMoV13of the untreated and nitride samples.

**Fig. 10.**The SEM morphologies of wear track of: (a) untreated sample, (b) nitrided sample.



 

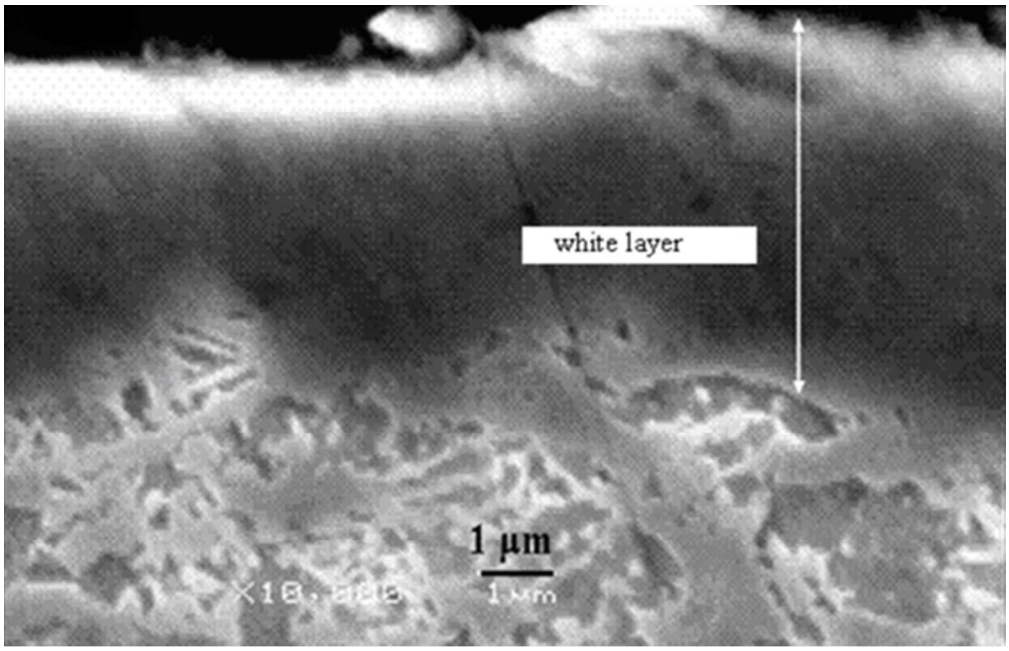


173x111mm (96 x 96 DPI)

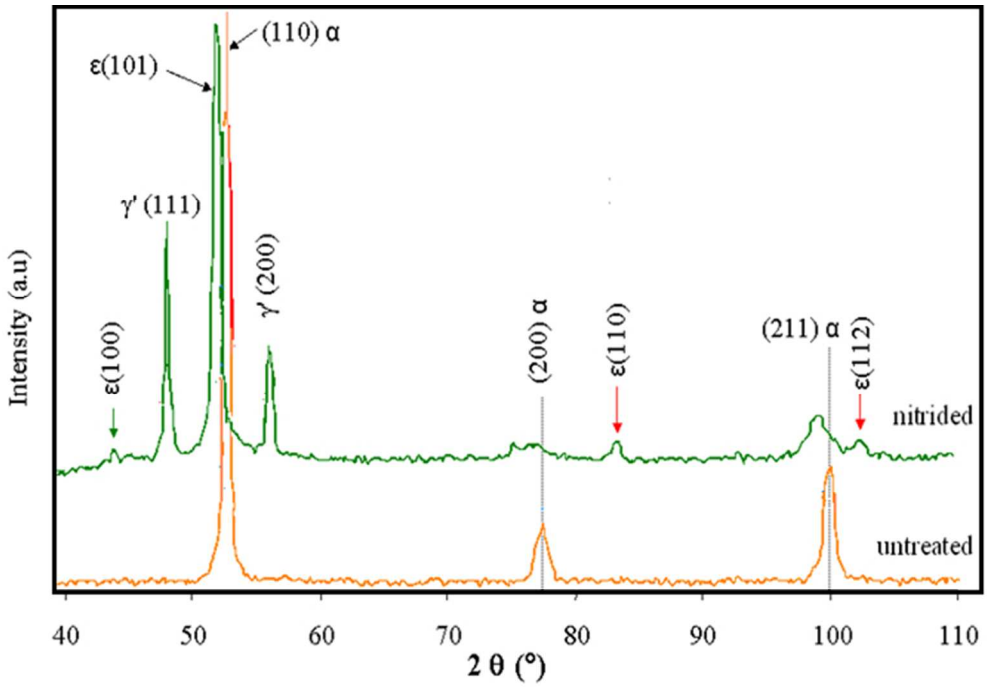


178x121mm (96 x 96 DPI)

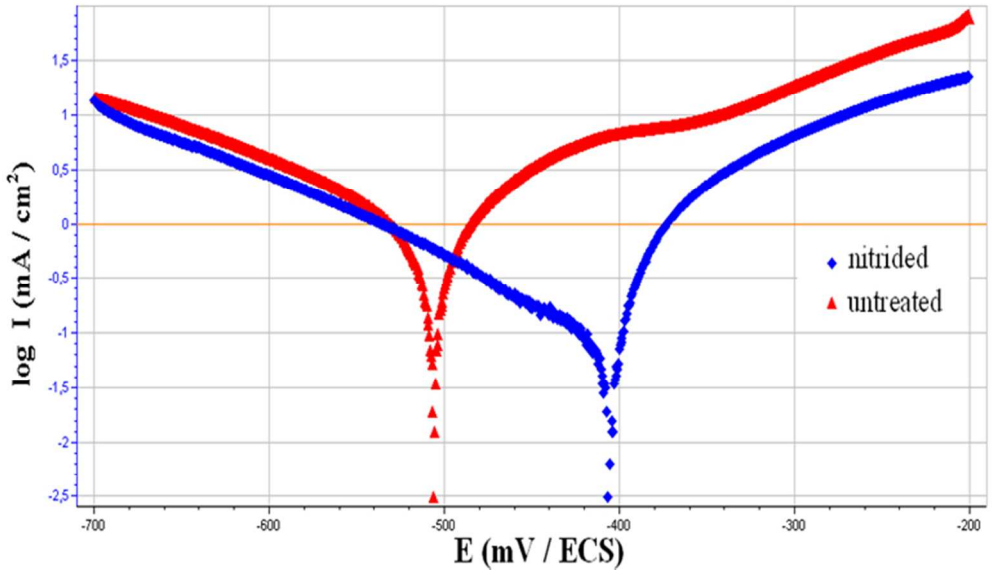


205x117mm (96 x 96 DPI)

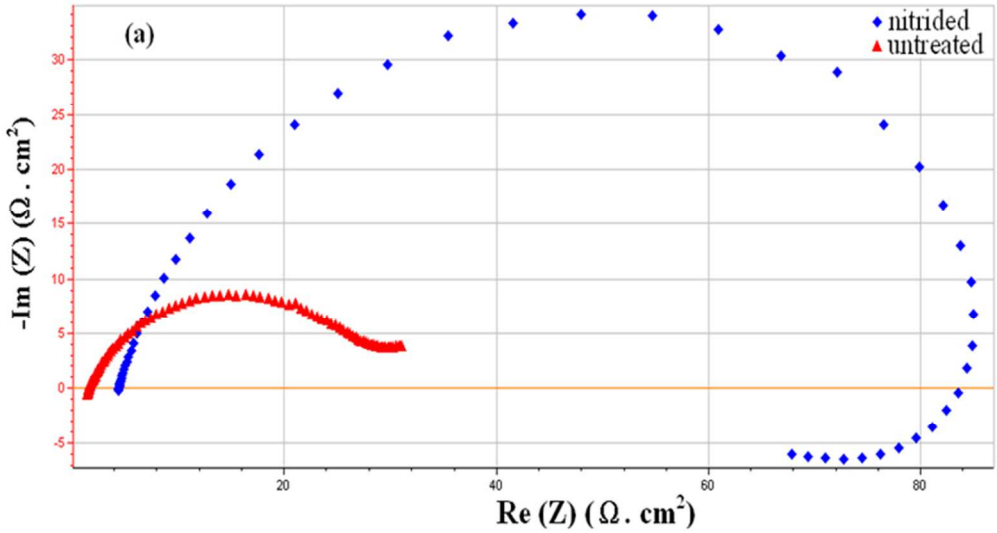


203x108mm (96 x 96 DPI)

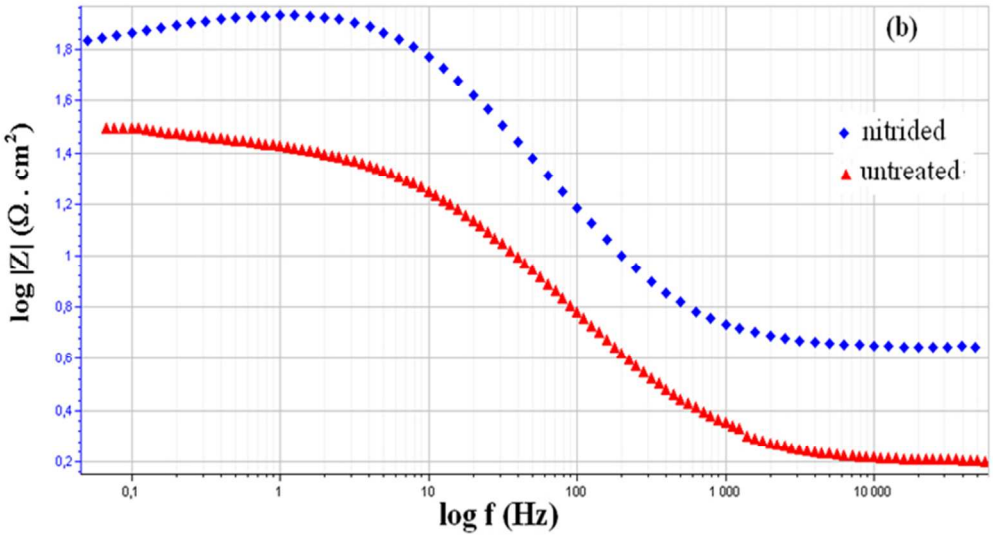


204x110mm (96 x 96 DPI)

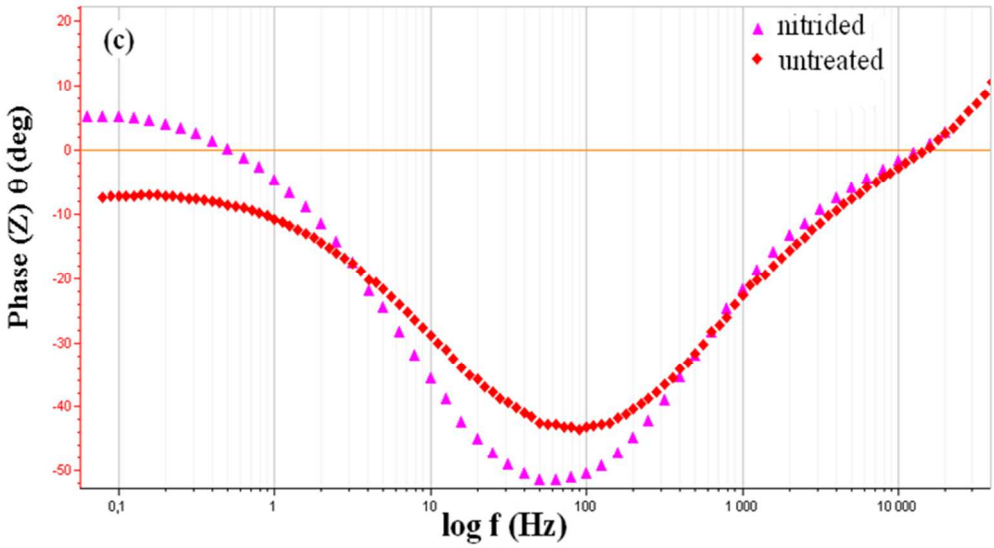


205x111mm (96 x 96 DPI)

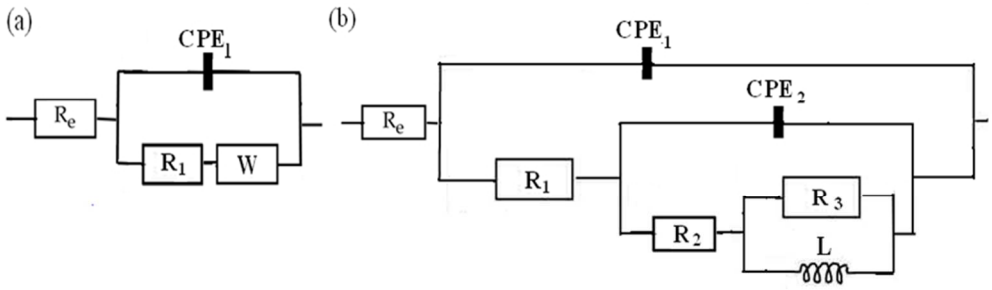


237x68mm (96 x 96 DPI)

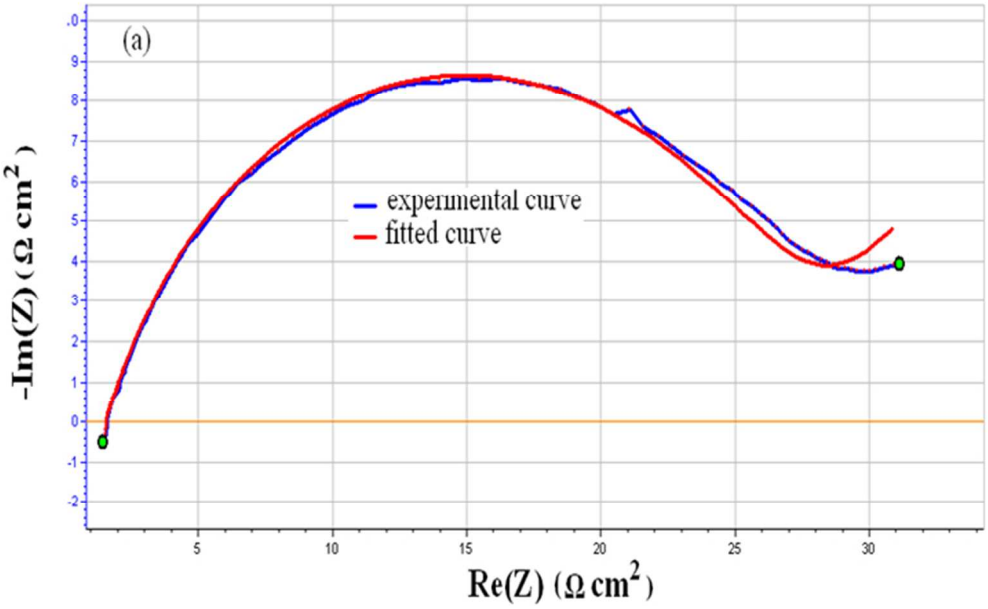


192x117mm (96 x 96 DPI)

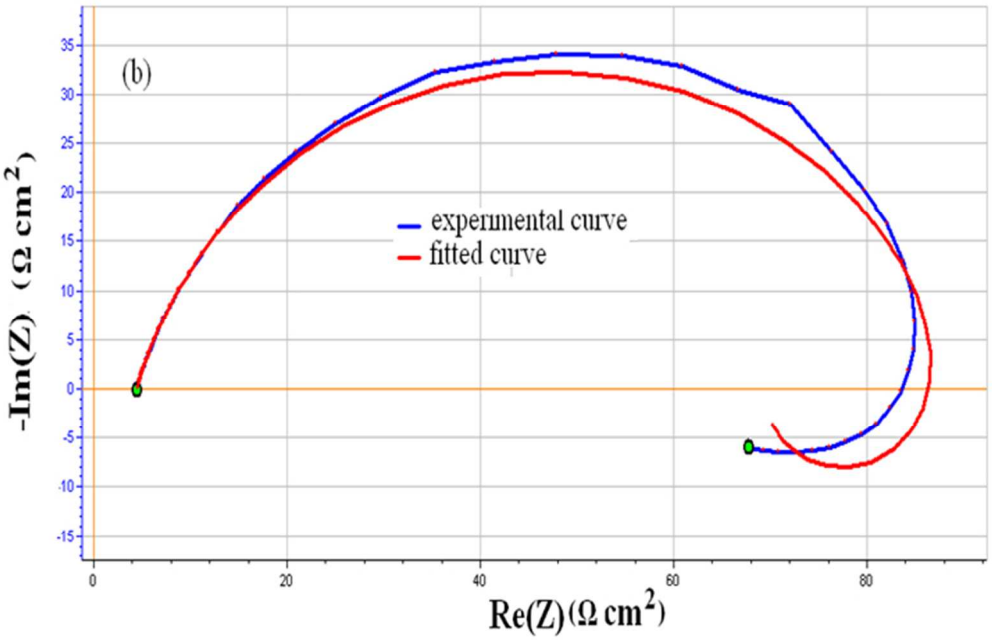


190x122mm (96 x 96 DPI)

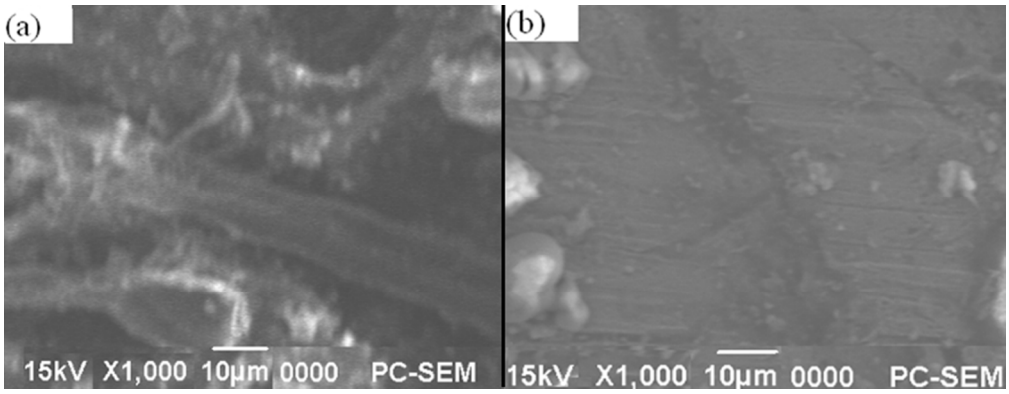


228x87mm (96 x 96 DPI)

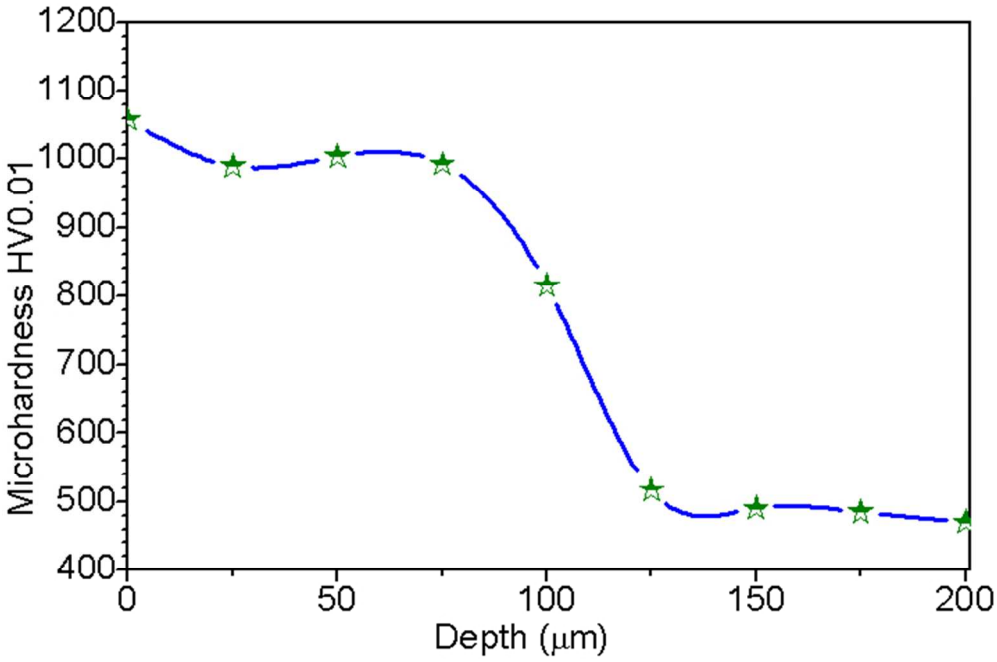


190x125mm (96 x 96 DPI)

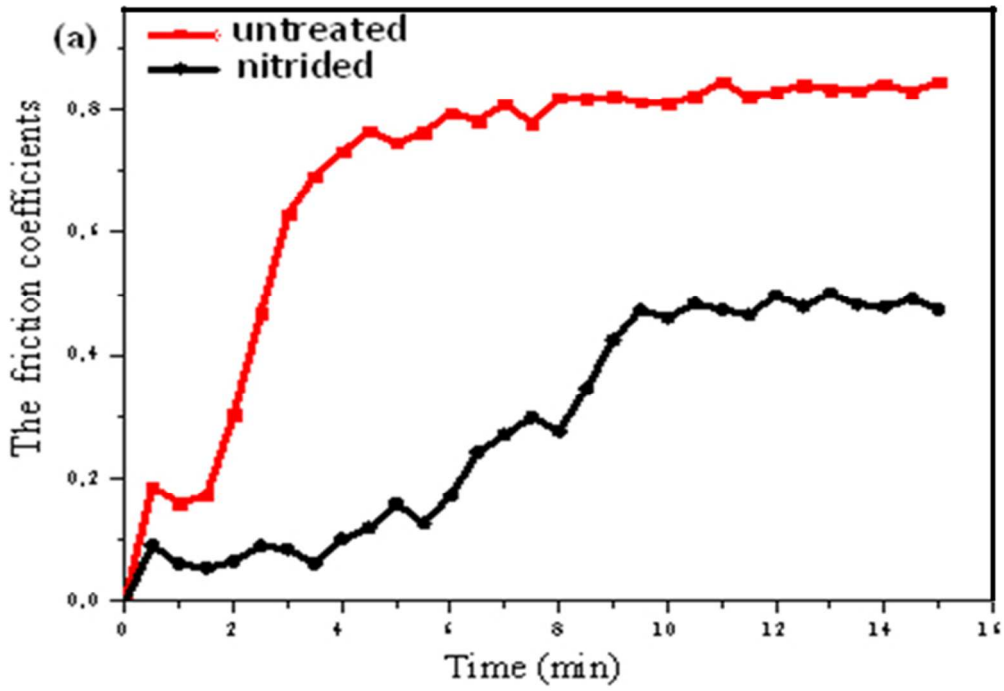


166x114mm (96 x 96 DPI)

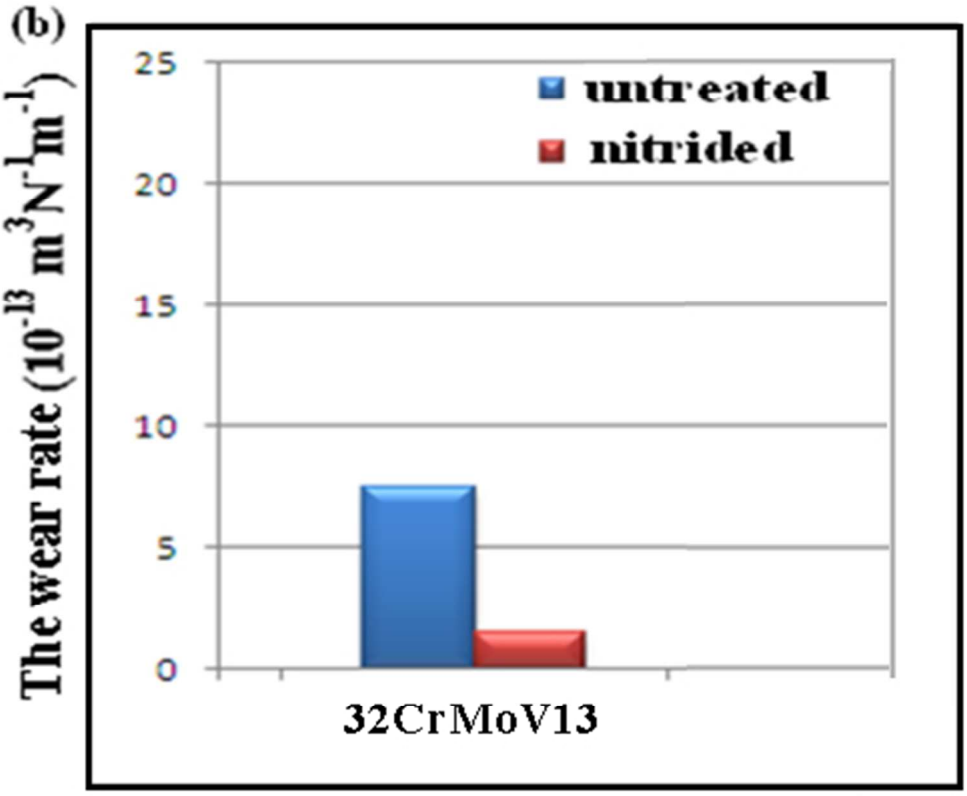


130x107mm (96 x 96 DPI)

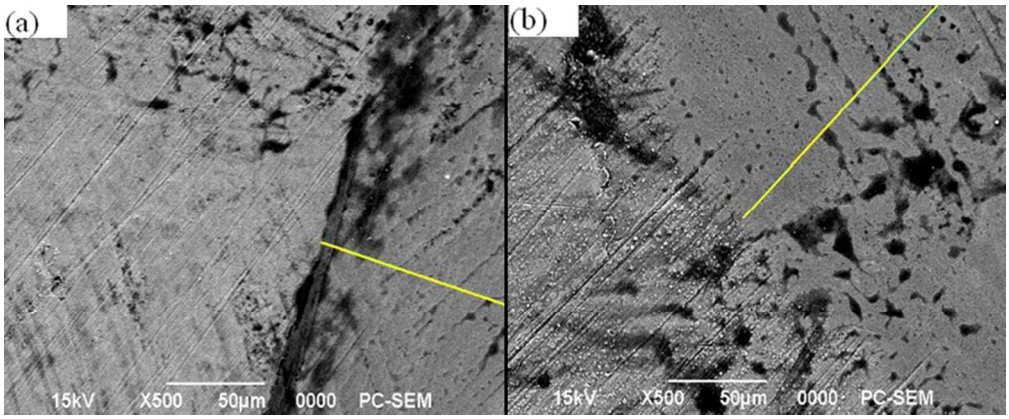


241x98mm (96 x 96 DPI)